J. Fluid Mech. (2004), *vol.* 518, *pp.* 125–145.
DOI: 10.1017/S002211200400103X Printed in the United Kingdom

Flow of a compressible fluid in a rapidly rotating pipe with azimuthally varying wall thermal condition

By JUN SANG PARK[1] AND JAE MIN HYUN[2]†

[1]Department of Mechanical Engineering, Halla Institute of Technology, San 66, HeungUp, Wonju, Kangwondo 220-712, South Korea

[2]Department of Mechanical Engineering, Korea Advanced Institute of Science and Technology, 373-1 Kusong-Dong, Yusung-gu, Taejon 305-701, South Korea

(Received 1 September 2003 and in revised form 15 May 2004)

An analysis is made of steady-state flow of a compressible fluid in an infinite rapidly rotating pipe. Flow is induced by imposing a small azimuthally varying thermal forcing at the pipe wall. The Ekman number is small. Analyses are conducted to reveal both the axisymmetric-type and non-axisymmetric-type solutions. The axisymmetric solution is based on the azimuthally averaged wall boundary condition. The non-axisymmetric solution stems from the azimuthally fluctuating part of the wall boundary condition. It is shown that the two-dimensional (uniform in the axial direction) non-axisymmetric solution exists for $\sigma(\gamma-1)M^2 \gg O(E^{1/3})$. However, an axially dependent solution is found if $\sigma(\gamma-1)M^2 \lesssim O(E^{1/3})$, in which E denotes the Ekman number, M the Mach number, γ the specific heat ratio and σ the Prandtl number. The axisymmetric solution prevails over the whole flow region; the two-dimensional non-axisymmetric solution is confined to the near-wall thermal layer of thickness $O(E^{1/3})$. As a canonical example, a detailed description is given for the case of a highly conducting wall with differential heating.

1. Introduction

This paper reports an analytical description of steady flow of a compressible fluid contained in a rapidly rotating infinitely long cylindrical pipe of radius D^*. The usual cylindrical frame (r^*, θ, z^*) is adopted [see figure 1]. In the basic state, the pipe and the gas, which rotate steadily about the z^*-axis at constant rotation rate Ω^*, are in thermal equilibrium at constant temperature T^*_{00}. Here, the rotation rate Ω^* is sufficiently high that the fluid compressibility effect, as represented by finite values of the peripheral Mach number M, is significant. The gas in the pipe is in rigid-body rotation, and the density increases exponentially in the radially outward direction (e.g. Sakurai & Matsuda 1974; Nakayama & Usui 1974; Bark & Bark 1976; Park & Hyun 2001). Departures from the rigid-body rotation are created by imposing a small temperature perturbation on the pipe wall, and the resulting flow is the subject of the present investigation. The problem is relevant to industrial applications of high-speed rotating-fluid machinery (e.g. Torri & Yang 1994) and to the models of astrophysical systems (e.g. Gans 1975; Matsuda 1983). These flows are characterized

† Author to whom correspondence should be addressed: jmhyun@kaist.ac.kr.

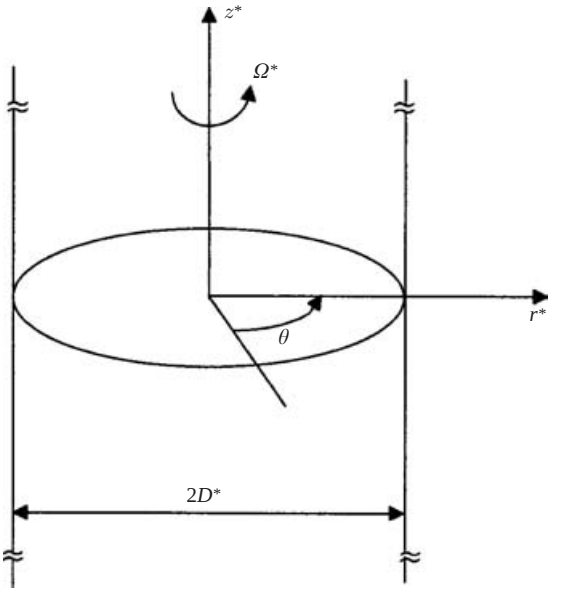

FIGURE 1. Problem configuration.

by the smallness of the system Ekman number, $E[\equiv\mu/\rho^*_{00}(D^*)\Omega^* D^{*2}] \ll 1$, in which μ is the coefficient of viscosity, $\rho^*_{00}(D^*)$ the fluid density at the wall. The present problem poses issues pertinent to the basic behaviour of rapidly rotating compressible fluid flow (e.g. Frankel 1959; Morton & Shaughnessy 1972; Gans 1974; Sakurai & Matsuda 1974; Lalas 1975; Matsuda, Hashimoto & Takeda 1976; Louvet & Durivault 1977; Bark & Hultgren 1979; Miles 1981; Hyun & Park 1989; Park & Hyun 1989, 1990; Babarsky, Herbst & Wood 2002).

Park & Hyun (2001) dealt with the flow which arises in response to the imposition of an axisymmetric thermal forcing at the pipe wall. Also, the assumption of heavy-gas limit ($\gamma = 1.0$, γ being the ratio of specific heats) was invoked for small Mach number, $M \ll 1.0$. The purpose of the present paper is to relax these restrictive assumptions, i.e. in the present work, the thermal forcing at the wall is taken to be an arbitrary function of the azimuthal coordinate θ. As emphasized, the specific heat ratio and the Mach number are now assumed to be $(\gamma - 1) \sim O(1)$ and $M \sim O(1)$. Theoretical approaches are pursued for the steady-state situation, and the outcome demonstrates that substantial qualitative differences exist between the results of the preceding analysis (Park & Hyun 2001) and the present effort.

One key dynamic ingredient of the boundary-layer flow under a non-axisymmetric (θ-dependent) forcing is the $E^{1/3}$-thermal layer. This was explored by Matsuda & Nakagawa(1983) in a pie-shaped cylinder of infinite length rotating about the apex. This layer plays a role of matching the axisymmetric temperature field in the interior to the θ-dependent temperature condition at the wall. Wood & Babarsky (1992) extended the analysis to describe the cylindrical 'pancake' layer. In the present study, it is stressed that the container is an axisymmetric pipe, but the forcing at the wall is taken to be a general function of the azimuthal angle θ.

The major findings of the present theoretical endeavours are summarized here. For a compressible fluid, under a non-axisymmetric thermal forcing at the wall, the temperature in the interior is substantially axisymmetric for $\sigma(\gamma - 1)M^2 \gg O(E^{1/3})$,

where σ is the Prandtl number. The impact of the non-axisymmetric part of the thermal loading at the wall is absorbed in the $E^{1/3}$-thermal layer adjacent to the wall. This induces a closed circulation in the $E^{1/3}$-thermal layer, which, in turn, gives rise to generation (removal) of heat by compression (expansion) work of the radial flows. For $\sigma(\gamma-1)M^2 \lesssim O(E^{1/3})$, a fully ($z$-dependent) three-dimensional flow is seen.

The aforestated features are in contrast to the case of an incompressible fluid. In the latter, a non-axisymmetric thermal forcing at the wall produces a corresponding non-axisymmetric temperature field in the interior. This can be easily understood since, for the latter, the governing equation is the diffusion equation (see Carslaw & Jaeger 1959; Batchelor 1967).

In the present paper, the mathematical formulation is posed in § 2. Theoretical analyses are undertaken in § 3. Physical rationalizations are given in § 4, and illustrative examples are presented. Concluding remarks are given in § 5.

2. Problem formulation

The flow geometry is sketched in figure 1. The cylindrical coordinates (r^*, θ, z^*), with the corresponding velocity components (u^*, v^*, w^*), are selected. The solid wall of the pipe ($r^* = D^*$) is assumed isothermal.

For a perfect gas, the density field in the basic-state rigid-body rotation is given as (e.g. Bark & Bark 1976)

$$\rho^*_{00}(r^*) = \rho^*_{00}(D^*)\exp\left[\tfrac{1}{2}\gamma M^2(r^2-1)\right], \tag{1}$$

in which subscript 00 refers to the undisturbed basic state at uniform temperature T^*_{00}, and M is the Mach number of the peripheral velocity at the wall, $M \equiv \Omega^* D^*/(\gamma R T^*_{00})^{1/2}$, R the gas constant, and $r \equiv r^*/D^*$. The superscript * denotes dimensional quantities. Equation (1) indicates that the density increases exponentially in the radially outward direction.

Now, a small deviation from the above rigid-body rotation, by imposing a thermal perturbation at the wall, is considered. The magnitude of the perturbation is gauged by the Rossby number $\varepsilon \equiv T^p/T^*_{00}$, where T^p stands for the size of the thermal perturbation in the system. It is, therefore, advantageous to implement a consistent scheme of non-dimensionalization, which is guided by the preceding studies (e.g. Sakurai & Matsuda 1974; Park & Hyun 2001):

$$u = \frac{\gamma M^2 u^*}{\varepsilon \Omega^* D^*}, \quad v = \frac{\gamma M^2 v^*}{\varepsilon \Omega^* D^*}, \quad p = \frac{p^*}{\varepsilon \rho^*_{00}(D^*) R T^*_{00}},$$
$$T = \frac{T^*}{\varepsilon T^*_{00}}, \quad \rho = \frac{\rho^*}{\varepsilon \rho^*_{00}(D^*)}, \quad t = t^* \Omega^*.$$

In the above, ρ^*, p^* and T^* denote the dimensional perturbations of density, pressure and temperature, respectively.

The governing non-dimensional linearized steady Navier–Stokes equations, viewed on the cylindrical frame rotating at Ω^*, are (e.g. Bark & Bark 1976; Bark & Hultgren 1979; Park & Hyun 2001):

$$\frac{1}{r}\frac{\partial}{\partial r}(r\rho_{00}u) + \frac{1}{r}\frac{\partial}{\partial \theta}(\rho_{00}v) = 0, \tag{2}$$

$$-2\rho_{00}v - \gamma M^2 r\rho = -\frac{\partial p}{\partial r} + E\left[\left(\nabla^2 - \frac{1}{r^2}\right)u + \left(\tfrac{1}{3}+\beta\right)\frac{\partial}{\partial r}(\nabla\cdot\boldsymbol{u}) - \frac{2}{r^2}\frac{\partial v}{\partial \theta}\right], \tag{3}$$

$$2\rho_{00}u + \frac{1}{r}\frac{\partial p}{\partial \theta} = E\left[\left(\nabla^2 - \frac{1}{r^2}\right)v + \frac{1}{3r}\frac{\partial}{\partial \theta}\nabla\cdot\boldsymbol{u} + \frac{2}{r^2}\frac{\partial u}{\partial \theta}\right], \tag{4}$$

$$-\frac{\sigma(\gamma-1)}{\gamma}r\rho_{00}u = E\nabla^2 T, \tag{5}$$

$$p = \rho + \rho_{00}T, \tag{6}$$

in which

$$\nabla^2 = \frac{\partial^2}{\partial r^2} + \frac{1}{r}\frac{\partial}{\partial r} + \frac{1}{r^2}\frac{\partial^2}{\partial \theta^2},$$

and β is the ratio of the expansion and shear viscosities, and the Prandtl number $\sigma \equiv \mu C_p/k$, μ is the coefficient of viscosity, C_p is the specific heat at constant pressure and k is the coefficient of thermal conductivity. The basic-state density field, in non-dimensional form, can be written as $\rho_{00}(r) \equiv \exp[\frac{1}{2}\gamma M^2(r^2-1)]$.

In the present problem formulation, the thermal forcing at the wall is prescribed to be an arbitrary function of azimuthal coordinate, i.e. $f(\theta)$. Accordingly, the boundary conditions are:

$$u(r=1.0,\theta)=0, \quad v(r=1.0,\theta)=0, \quad T(r=1.0,\theta)=f(\theta). \tag{7}$$

It is convenient to deploy a circumflex to represent the azimuthally averaged value of a dependent variable, i.e.

$$\hat{\phi} = \frac{1}{2\pi}\int_{-\pi}^{\pi}\phi(r,\theta)\,\mathrm{d}\theta. \tag{8a}$$

Furthermore, a tilde denotes the deviation of ϕ from $\hat{\phi}$, i.e.

$$\tilde{\phi} = \phi(r,\theta) - \hat{\phi}. \tag{8b}$$

It follows immediately that the thermal forcing at the wall in (7) can be decomposed into axisymmetric and non-axisymmetric parts:

$$f(\theta)[\equiv T(r=1,\theta)] = \hat{f} + \sum_n \tilde{f}_n\,\mathrm{e}^{\mathrm{i}n\theta},$$

where the index n refers to the nth complex Fourier component

$$\tilde{f}_n = \frac{1}{2\pi}\int_{-\pi}^{\pi} f(\theta)\,\mathrm{e}^{-\mathrm{i}n\theta}\,\mathrm{d}\theta.$$

Equation (7) can then be re-expressed as:
(for the axisymmetric part)

$$\hat{u}(r=1.0,\theta)=0, \quad \hat{v}(r=1.0,\theta)=0, \quad \hat{T}(r=1.0,\theta)=\hat{f}, \tag{9a}$$

(for the non-axisymmetric part)

$$\tilde{u}(r=1.0,\theta)=0, \quad \tilde{v}(r=1.0,\theta)=0, \quad \tilde{T}(r=1,\theta)=\sum_n \tilde{f}_n\,\mathrm{e}^{\mathrm{i}n\theta}. \tag{9b}$$

3. Analysis

3.1. *Axisymmetric part*

The velocity and temperature fields in the steady state, subject to an axisymmetric thermal forcing, i.e. $T_w = \hat{f}$, are now delineated (see (8a)). The subscript w refers to the

pipe wall at $r = 1.0$. By employing the averaging process (see (8*a*)) to the continuity equation, (2), the axisymmetric radial velocity is

$$\hat{u}_s(r) = 0. \tag{10}$$

Here, subscript s refers to the steady state. Substituting (10) into the azimuthally averaged forms of (4) and (5) yields

$$\hat{v}_s(r) = 0, \tag{11}$$

$$\hat{T}_s(r) = \hat{f}. \tag{12}$$

Obviously, the above results reconfirm that the steady-state flow is in isothermal rigid-body rotation.

The associated density and pressure fields can be found by undergoing algebraic manipulations. From (6), we have,

$$\hat{p}_s(r) = \hat{\rho}_s(r) + \rho_{00}(r)\hat{f}. \tag{13}$$

Bringing (13) into the axisymmetric part of (3) produces

$$\frac{\mathrm{d}\hat{\rho}_s}{\mathrm{d}r} - \gamma M^2 r \hat{\rho}_s = -\hat{f}\,\frac{\mathrm{d}\rho_{00}}{\mathrm{d}r}. \tag{14}$$

The solution to (14) is found to be

$$\hat{\rho}_s(r) = \left(C_1 - \tfrac{1}{2}\hat{f}\gamma M^2 r^2\right)\rho_{00}(r). \tag{15}$$

The integration constant C_1 is determined by using the global mass continuity, i.e. $\int_0^1 \hat{\rho}_s 2\pi r\,\mathrm{d}r = 0$:

$$C_1 = \tfrac{1}{2}\hat{f}\left(\frac{\gamma M^2}{1 - \exp(-\gamma M^2/2)} - 2\right).$$

The pressure $\hat{p}_s$ is obtained from (13):

$$\hat{p}_s(r) = \tfrac{1}{2}\hat{f}\gamma M^2\left(\frac{1}{1 - \exp(-\gamma M^2/2)} - r^2\right)\rho_{00}(r). \tag{16}$$

Compiling the above developments, the steady-state density and pressure profiles, subject to the axisymmetric thermal forcing $T_w = \hat{f}$, are illustrated. As seen in figure 2(*a*), for $\hat{f} > 0$, in comparison with the basic state, density is larger (smaller) in the interior region near the axis (near the wall). (For $\hat{f} < 0$, the trend is reversed.) It is noted that, in the steady state, the temperatures of the fluid and of the wall are equalized. Therefore, the effective peripheral Mach number is smaller (larger) than that of the basic state for $\hat{f} > 0$ ($\hat{f} < 0$). It is recalled that, when the rotational speed of the pipe wall is unchanged, the peripheral Mach number is inversely proportional to the acoustic speed ($a = \sqrt{\gamma R T_w}$). In the case of isothermal rigid-body rotation, the radial profile of density $\rho_s(r)$, as shown in (15), is determined by γ and M, and the radial variation of $\rho_s(r)$ becomes steeper (milder) as M increases (decreases). This explanation is in accord with the above characterization of $\rho_s(r)$.

The pressure profile, as displayed in figure 2(*b*), is similar to the density profile. However, the qualitative difference between the two profiles is also notable. Unlike $\hat{\rho}_s(r)$, for $\hat{f} > 0$ ($\hat{f} < 0$), the pressure is higher (lower) than the corresponding basic-state value throughout the entire region. A proper physical interpretation is in order. As is evident in (13), the pressure profile is determined by both the density [$\hat{\rho}_s(r)$] and temperature ($\hat{f}$). For $\hat{f} > 0$, in the central interior region, both the density and

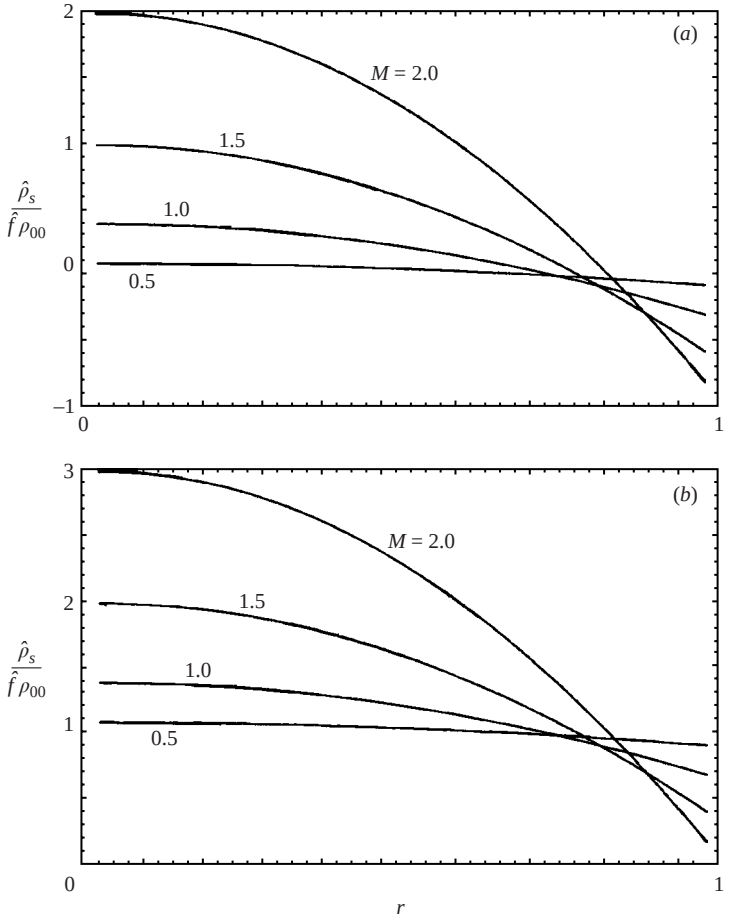

FIGURE 2. Axisymmetric fields of (*a*) density $\hat{\rho}_s$ and (*b*) pressure $\hat{p}_s$. $\gamma = 1.4$.

temperature increase, which causes the pressure to increase. However, for $\hat{f} > 0$, near the wall, the density decreases but the temperature increases, which makes opposite contributions to the change in pressure. In this case, the pressure increase due to the temperature increase outweighs the pressure decrease due to the density decrease (this can be readily confirmed by inspecting (13) and (15)). In summary, if $\hat{f} > 0$ ($\hat{f} < 0$), the steady-state pressure is larger (smaller) than the basic-state value in the entire region.

It is worth mentioning that the Ekman number E and Prandtl number σ do not enter in the determination of the axisymmetric flow and temperature fields. Therefore, the values of E and σ are not given in the caption of figure 2.

It is of interest to examine the profiles of density and pressure in the two limiting cases, i.e. $M \ll 1$ and $M \gg 1$.

(i) $M \ll 1$ (the incompressible-flow limit)

From (15) and (16), for $M \ll 1$, we have

$$\hat{\rho}_s \sim O(M^2), \tag{17a}$$

$$\hat{p}_s \cong \hat{f} + O(M^2). \tag{17b}$$

It implies that the density field for $M \ll 1$ is uniform and infinitesimally different from the basic-state value throughout the whole region within the error bound of $O(M^2)$. The perturbed pressure field $\hat{p}_s$ is also nearly uniform in the entire region, and, owing to the temperature increase at the wall $\hat{f}$, the increase of pressure over the baisc-state value is $\hat{p}_s/\hat{f} = 1$. Alternatively stated, in the incompressible-flow limit ($M \ll 1$), an alteration in fluid temperature causes a change only in pressure, not in density. This assertion, as demonstrated in figure 2(*a*), is consistent with the earlier finding of Park & Hyun (2001) for the heavy gas limit.

(ii) $M \gg 1$(the hypersonic flow limit)

If $M \gg 1$, (15) and (16) can be approximated:

$$\hat{\rho}_s \cong \hat{f}\left[\tfrac{1}{2}\gamma M^2(1-r^2)-1\right]\rho_{00} + O(M^2\exp(-M^2)), \tag{18a}$$

$$\hat{p}_s \cong \hat{f}\left(\tfrac{1}{2}\gamma M^2\right)(1-r^2)\rho_{00} + O(M^2\exp(-M^2)). \tag{18b}$$

It is seen that, for $M \gg 1$, by the imposition of axisymmetric temperature increase at the wall $T_w = \hat{f}$, the perturbed density $[\hat{\rho}_s/\rho_{00}]$ and pressure $[\hat{p}_s/\rho_{00}]$ profiles become quadratic in r. It is useful to locate the radial position R_c at which the density variation reaches zero, $\hat{\rho}_s = 0$:

$$R_c = \sqrt{1 - \frac{2}{\gamma M^2}}. \tag{19}$$

The physical meaning of this characteristic radial distance R_c is clear. In $0 \leqslant r < R_c$, the correlation between changes in density and temperature is positive ($\hat{\rho}_s/\hat{f}\rho_{00} > 0$); and in $R_c < r \leqslant 1$, the correlation is negative ($\hat{\rho}_s/\hat{f}\rho_{00} < 0$). Moreover, from (13), the effects of temperature and of density on the pressure distribution are cooperative in $0 \leqslant r < R_c$ and opposing in $R_c < r \leqslant 1$. These interpretations are in line with the prior physical explanations on figure 2(*b*). Consequently, in the case of $M \gg 1$, the entire flow region is separated into qualitatively different regions: the cooperative zone, $0 \leqslant r < R_c$ and the opposing zone, $R_c < r \leqslant 1$.

A perusal of (19) is made for the situation of very large M, i.e. $R_c \to 1.0$ when $M \to \infty$. In this case, the cooperative zone prevails in the entire region with the exception of $r = 1$, in which changes in both density and pressure are positively correlated in $0 \leqslant r < 1$ with the imposed change in wall temperature. Physically speaking, in the limit $M \gg 1$, the majority of the mass of rotating fluid is concentrated in the immediate neighbourhood of the wall ($r = 1$). It then follows that most of the total thermal energy transferred between the fluid and the wall is restricted to a thin opposing zone adjacent to the wall. As $M \to \infty$, the opposing zone, $R_c < r \leqslant 1$, shrinks rapidly to the vicinity of the wall. In this extremely narrow region, as stipulated, the density decreases (increases) owing to volumetric expansion (compression) of the fluid, which is caused by the heating (cooling) at the wall. Therefore, in nearly the entire region, i.e. cooperative zone, $0 \leqslant r < R_c$ when $R_c \to 1.0$, the fluid is compressed (expanded) with the heating (cooling) at the wall so that both density and pressure increase (decrease) (see figure 2*b*).

3.2. *Non-axisymmetric part*

Now, analyses are made of the interior flow when the thermal forcing at the wall is non-axisymmetric. It will be shown that z-independent solutions are permitted only under the condition $\sigma(\gamma-1)M^2 \gg O(E^{1/3})$. When this condition is not satisfied, i.e. $\sigma(\gamma-1)M^2 \lesssim O(E^{1/3})$, the flow is z-dependent, which implies full three-dimensionality of the interior flow. This will be derived as part of the solution procedures.

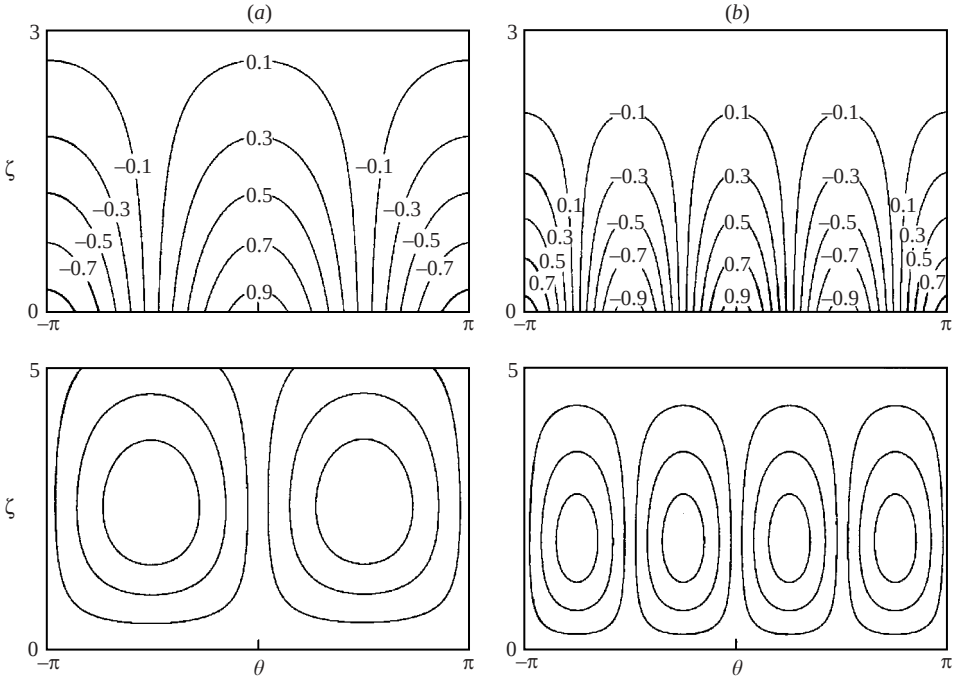

FIGURE 3. Plots of harmonic components for non-axisymmeric temperature fields (top frame) and stream functions (bottom frame). $M = 1.0$, $\gamma = 1.4$, $\sigma = 0.7$. $\Delta\Psi = 0.3$. (*a*) $n = 1$; (*b*) $n = 2$.

3.2.1. *z-independent flow for* $\sigma(\gamma - 1)M^2 \gg O(E^{1/3})$

The crux of the argument is that, when $\sigma(\gamma - 1)M^2 \gg O(E^{1/3})$, the impact of the non-axisymmetric thermal forcing at the wall can be effectively absorbed within the sidewall thermal layer of thickness $O(E^{1/3})$, which is similar to the well-known $E^{1/3}$-sidewall Stewartson layer (see Sakurai & Matsuda 1974; Bark & Bark 1976) and to the thermal layer depicted by Matsuda & Nakagawa (1983) and Wood & Babarsky (1992). In the bulk of the interior, $0 \leqslant r < 1 - O(E^{1/3})$, the flow is substantially axisymmetric, which is induced by the axisymmetric forcing at the wall.

For $E \ll 1$, to secure a meaningful asymptotic solution, the flow variables are expanded as

$$\tilde{\Phi} = \sum_{n=0}^{\infty} E^{n/m} \tilde{\Phi}_n(\zeta, \theta),$$

in which $\zeta = (1 - r)/E^{1/m}$ and $\tilde{\Phi}$ denotes $\tilde{u}$, $\tilde{v}$, $\tilde{\rho}$, $\tilde{p}$ or $\tilde{T}$. Upon substituting the above expansions into the non-axisymmetric parts of governing equations (2)–(6), we can easily find a choice of $m = 3$ and $\tilde{u}_0 = \tilde{p}_0 = 0$. Therefore, the problem has a proper expansion parameter $E^{1/3}$ and the associated boundary-layer coordinate $\zeta = (1 - r)/E^{1/3}$. The leading-order dependent variables are scaled as

$$\tilde{u}_s \sim O(E^{1/3}), \quad \tilde{v}_s \sim O(1), \quad \tilde{T}_s \sim O(1), \quad \tilde{\rho}_s \sim O(1), \quad \tilde{p}_s \sim O(E^{1/3}).$$

In the above, a tilde refers to the non-axisymmetric component and subscript s to the steady solution. The above scalings are similar to those for the $E^{1/3}$-Stewartson layer (Bark & Bark 1976) and to the $E^{1/3}$-thermal layer (Matsuda & Nakagawa 1983; Wood & Babarsky 1992).

The leading-order governing equations are, from (2)–(6),

$$-\frac{\partial \tilde{u}_s}{\partial \zeta} + \frac{\partial \tilde{v}_s}{\partial \theta} = 0, \tag{20a}$$

$$2\tilde{v}_s + \gamma M^2 \tilde{\rho}_s + \frac{\partial \tilde{p}_s}{\partial \zeta} = 0, \tag{20b}$$

$$2\tilde{u}_s + \frac{\partial \tilde{p}_s}{\partial \theta} - \frac{\partial^2 \tilde{v}_s}{\partial \zeta^2} = 0, \tag{20c}$$

$$\frac{\sigma(\gamma-1)}{\gamma}\tilde{u}_s + \frac{\partial^2 \tilde{T}_s}{\partial \zeta^2} = 0, \tag{20d}$$

$$\tilde{\rho}_s + \tilde{T}_s = 0. \tag{20e}$$

From (20*b*), (20*c*) and (20*e*), we have

$$\gamma M^2 \frac{\partial \tilde{T}_s}{\partial \theta} = \frac{\partial^3 \tilde{v}_s}{\partial \zeta^3}, \tag{21a}$$

and, from (20*a*) and (20*d*),

$$-\frac{\sigma(\gamma-1)}{\gamma}\frac{\partial \tilde{v}_s}{\partial \theta} = \frac{\partial^3 \tilde{T}_s}{\partial \zeta^3}. \tag{21b}$$

By eliminating $\tilde{v}$ from (21*a*) and (21*b*), the equation for temperature is obtained:

$$\frac{\partial^6 \tilde{T}_s}{\partial \zeta^6} + \sigma(\gamma-1)M^2 \frac{\partial^2 \tilde{T}_s}{\partial \theta^2} = 0. \tag{22}$$

It is apparent that, in view of the above scalings, the solution of (22) is meaningful for the parameter range $\sigma(\gamma-1)M^2 \sim O(1)$, i.e. $\sigma(\gamma-1)M^2 \gg O(E^{1/3})$. In addition, it is worth mentioning that (22) was also derived by Matsuda & Nakagawa (1983), who investigated gas flows in a pie-shaped infinitely long cylinder rotating about the apex.

The appropriate boundary conditions for (22) are:

$$\text{at } \zeta = 0, \quad \tilde{T}_s = \sum_n \tilde{f}_n \, \mathrm{e}^{\mathrm{i}n\theta}, \tag{23a}$$

$$\frac{\partial^2 \tilde{T}_s}{\partial \zeta^2} = 0, \tag{23b}$$

$$\frac{\partial^3 \tilde{T}_s}{\partial \zeta^3} = 0, \tag{23c}$$

and, as $\zeta \to \infty$, all the variables tend to zero. Equation (23*a*) expresses the imposed thermal loading at the wall, and (23*b*) states the non-permeable condition at the wall, i.e. $\tilde{u}_s = 0$ leads to $\partial^2 \tilde{T}_s / \partial \zeta^2 = 0$ (see (20*d*)), and (23*c*) states the no-slip condition at the wall, i.e. $\tilde{v}_s = 0$ leads to $\partial^3 \tilde{T}_s / \partial \zeta^3 = 0$ (see (21*b*)).

In a manner similar to Sakurai & Matsuda (1974), the function $\tilde{T}$ is expanded as

$$\tilde{T}_s(\zeta, \theta) = \sum_n \tilde{T}_n(\zeta) \, \mathrm{e}^{\mathrm{i}n\theta}. \tag{24}$$

By substituting (24) into (22), the solution $\tilde{T}_n(\zeta)$, subject to (23*a*)–(23*c*), is acquired:

$$\tilde{T}_n(\zeta) = \tfrac{1}{2}\tilde{f}_n\left[\exp(-\gamma_n\zeta) + \exp(-\gamma_n\zeta/2)\frac{2}{\sqrt{3}}\cos\left(\frac{\sqrt{3}}{2}\gamma_n\zeta - \frac{\pi}{6}\right)\right], \tag{25}$$

in which $\gamma_n = (\sigma(\gamma-1)M^2n^2)^{1/6}$.

The radial and azimuthal velocities are given by (20*d*) and (21*b*):

$$\tilde{u}_s(\zeta,\theta) = -\frac{\gamma}{\sigma(\gamma-1)}\sum_n \tilde{U}_n(\zeta)\exp(\mathrm{i}n\theta), \tag{26}$$

$$\tilde{v}_s(\zeta,\theta) = -\frac{\gamma}{\sigma(\gamma-1)}\sum_n \tilde{V}_n(\zeta)\exp(\mathrm{i}(n\theta - \pi/2)), \tag{27}$$

in which

$$\tilde{U}_n(\zeta) = \tfrac{1}{2}\tilde{f}_n\gamma_n^2\left[\exp(-\gamma_n\zeta) + \frac{2}{\sqrt{3}}\exp(-\gamma_n\zeta/2)\sin\left(\frac{\sqrt{3}}{2}\gamma_n\zeta - \frac{\pi}{3}\right)\right],$$

$$\tilde{V}_n(\zeta) = -\frac{\tilde{f}_n}{2n}\gamma_n^3\left[\exp(-\gamma_n\zeta) + \frac{2}{\sqrt{3}}\exp(-\gamma_n\zeta/2)\sin\left(\frac{\sqrt{3}}{2}\gamma_n\zeta - \frac{2\pi}{3}\right)\right].$$

It is important to delineate the distinguishing features of the present endeavour as compared with the preceeding treatises (Sakurai & Matsuda 1974; Matsuda & Nakagawa 1983). As is discernible in (26) and (27), the $E^{1/3}$-thermal layer of strength $O(1)$ adjusts the non-axisymmetric temperature at the wall to the axisymmetric interior temperature field. Also, this layer satisfies both the no-slip and non-permeability conditions at the wall. It is to be noted that, unlike the previous studies, the thermal layer of the present study is a self-contained boundary layer.

In order to reinforce the above argument, the flow patterns of Matsuda & Nakawaga (1983) are shown in figure 4. They dealt with the steady-state flow in a rotating pie-shaped pipe. At two radial walls ($\theta =$ constant), different temperature T_{WU} and T_{WB} are imposed (say, $T_{WB} > T_{WU}$), and the cylindrical sidewall is highly conducting. It was shown that a buoyancy layer is developed near the radial wall, which is akin to the Ekman layer discussed in Sakurai & Matsuda (1974). Furthermore, an $E^{1/3}$-thermal layer is observed near the cylindrical sidewall, which is similar to the $E^{1/3}$-Stewartson layer. In the interior far away from the walls, the average temperature, $(T_{WU}+T_{WB})/2$, prevails. Also, a flow, $v \sim O(E^{1/2})$, exists which is directed from the relatively hot wall (T_{WU}) toward the cold wall (T_{WB}). In the $E^{1/3}$-thermal layer, a closed-path flow of leading order, $T \sim O(1)$, $v \sim O(1)$, $u \sim O(E^{1/3})$, is seen, which matches the interior to the temperature at the sidewall (see ② in figure). The resultant picture is that, in order to channel the mass flow of $O(E^{1/2})$ from a buoyancy layer to the opposite buoyancy layer (see flow path ① in figure), a first-order buoyancy-layer solution, $T \sim O(E^{1/6})$, $v \sim O(E^{1/6})$, $u \sim O(E^{1/2})$, is called for.

A straightforward extension of the Matsuda & Nakagawa (1983) to a case of arbitrary temperature distribution at the cylindrical wall brings forth both $E^{1/3}$- and $E^{1/4}$-thermal layers of $O(1)$. As pointed out by Heijst (1983), these leading-order $E^{1/3}$- and $E^{1/4}$-thermal layers call for the first-order solutions. Furthermore, in order to satisfy the no-slip condition, this solution entails complexities of a degenerate boundary layer, with the involvement of high-order solutions.

It is stressed here that the $E^{1/3}$-thermal layer of strength $O(1)$ of the present undertaking satisfies completely the velocity and temperature conditions. This capability stems from the shape of the container. The flow and thermal conditions in the

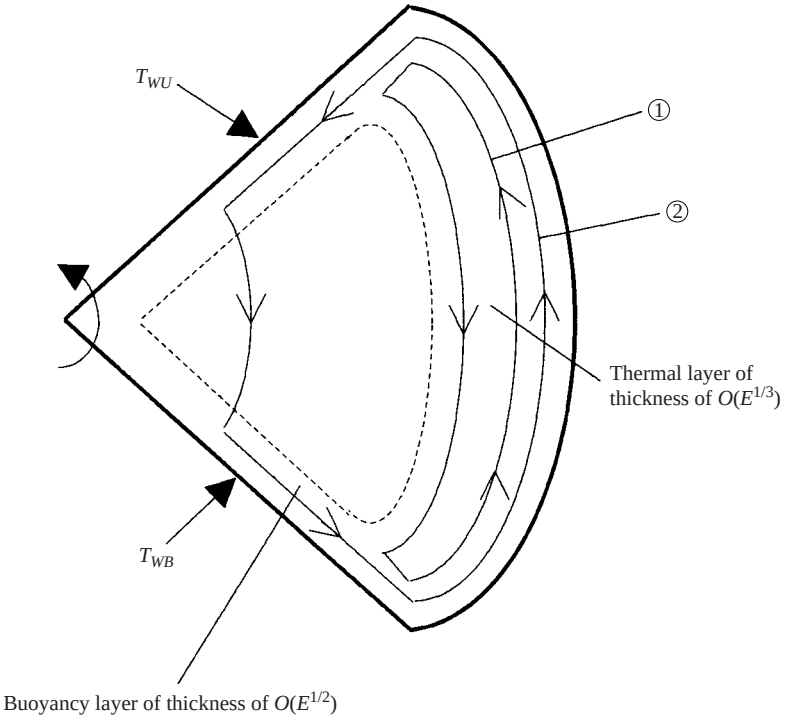

FIGURE 4. Schematic of the flow patterns in a pie-shaped cylinder of Matsuda & Nakagawa (1983).

interior are determined by the conditions at the radial walls in the case of a pie-shaped pipe of Matsuda & Nakagawa (1983). Similarly, these are determined by the rotating disk endwalls in the finite cylindrical container of Sakurai & Matsuda (1974). In the present problem of an infinite cylindrical pipe, the flow conditions in the interior are determined by the average temperature at the cylindrical wall. Thus, in the present formulation, there is no need for an $E^{1/4}$-thermal layer. It is noted that, in the geometry of Matsuda & Nakagawa (1983) the existence of buoyancy layers entails a mechanism of pumping the interior fluid to the $E^{1/3}$-thermal layer (in the case of Sakurai & Matsuda (1974) a similar role is played by the Ekman layer). However, in the present flow geometry, such a mechanism is absent, and there is no need to transport fluid from one buoyancy layer to another. Therefore, in the present geometry of axisymmetric cylindrical pipe, higher-order boundary layers are not called for.

In summary, for the present problem of an axisymmetric cylindrical pipe, the interior fluid is motionless at constant temperature. The $E^{1/3}$-thermal layer of strength of $O(1)$ near the wall absorbs completely the azimuthal variation of temperature imposed at the wall. These characteristics may be of relevance to futuristic space colonies (see Matsuda 1983).

The above theoretical developments offer succint physical interpretations. As shown in (22), when $\sigma(\gamma-1)M^2 \gg O(E^{1/3})$, the effect of non-axisymmetric thermal forcing at the wall is absorbed in the thermal layer of thickness $O(E^{1/3})$ adjacent to the wall. Inside the thermal layer, the fluid near the wall, where the thermal forcing is positive, i.e. in the azimuthal wall sector under heating, undergoes thermal expansion. This causes radially inward flows (see (26)). In contrast, in the azimuthal wall sector under

cooling, the fluid undergoes thermal compression, which generates radially outward flows. In response to the non-axisymmetric thermal condition at the wall, i.e. when the azimuthal wall sectors under heating and cooling coexist, the resulting radially inward and neighbouring radially outward flows induce azimuthal flows along the wall within this $O(E^{1/3})$-layer (see (26) and (27)). This is clear from the consideration of the continuity equation.

The overall picture inside this thermal layer is that, in the immediate vicinity of the wall, azimuthal flows are generated from a cool to a hot wall sector; in the far region away from the wall, azimuthal flows are in the opposite direction. These internal flows inside the layer create a closed circulation. In this process, the fluid experiences diffusive heating (cooling) from the hot(cold) sector of the wall. Simultaneously, the radially inward (outward)-moving fluid at the hot (cold) sector is cooled (heated) by the work done by the basic-state pressure field, i.e. $(\sigma(\gamma-1)/\gamma)\tilde{u}_s < 0$ $((\sigma(\gamma-1)/\gamma)\tilde{u}_s > 0)$, which is easily confirmed from the energy equation, (20*d*). This aspect is absent in the case of an incompressible fluid. For an incompressible fluid, the temperature field is governed by the diffusion equation. Therefore, a temperature disturbance at the wall is not confined within the $O(E^{1/3})$ boundary layer; the entire flow domain is directly influenced by the thermal boundary condition at the wall. This qualitative difference between compressible and incompressible flows was emphasized earlier by Matsuda *et al.* (1976).

In the present discussion for a rapidly rotating compressible fluid, under $\sigma(\gamma-1)M^2 \gg O(E^{1/3})$, the essential dynamical element is the generation of radial motions of $O(E^{1/3})$ owing to the imposition of non-axisymmetric thermal forcing at the wall (remember $\tilde{u}_s \sim O(E^{1/3})$). As represented by the first term of (20*d*), the radially inward (outward) motion causes volume expansion (compression) of the fluid element owing to the basic-state background pressure distribution given in (1), which results in cooling (heating) of the fluid. It is noted that the direct conductive heating (cooling) from the hot (cold) sector of the wall, represented by the second term of (20*d*), is offset by the cooling (heating) due to the aforesaid radial motions. Consequently, it is possible that the effect of non-axisymmetric thermal forcing at the wall is restricted within the $E^{1/3}$-thermal layer, rather than propagating to the entire flow domain approaching $r \to 0$.

The exemplary computed results of the above theoretical developments ((25)–(27)) are exhibited in figure 3 for the first ($n=1$) and second ($n=2$) modes. The temperature and velocity fields shown are fully supportive of the preceding assertions on the presence of a closed circulation within the $E^{1/3}$-layer. Similar results are obtainable for higher modes ($n \geqslant 3$).

In summary, when $\sigma(\gamma-1)M^2 \gg O(E^{1/3})$, the non-axisymmetric component of thermal forcing at the wall is absorbed within the $E^{1/3}$-thermal layer adjacent to the wall. In the interior region ($\zeta \to \infty$), only the effect of axisymmetric component of wall thermal forcing remains. This leads to the conclusion that, under the aforestated conditions, the temperature in the bulk of interior maintains axisymmetry even when a non-axisymmetric thermal boundary condition is imposed at the wall.

3.2.2. *Three-dimensional flow for* $\sigma(\gamma-1)M^2 \lesssim O(E^{1/3})$

It is recalled that, under $\sigma(\gamma-1)M^2 \lesssim O(E^{1/3})$, the previous scaling analysis of § 3.2.1 is no longer valid (see (22)). Physically, for $\sigma(\gamma-1)M^2 \lesssim O(E^{1/3})$, the compressibility of fluid is weak; thus, the radial motion in the boundary layer, which causes temperature variations of the fluid, is not strong enough to balance the thermal diffusion effect. This implies that a boundary-layer-type solution of order unity does

not exist. Therefore, the leading-order interior temperature itself has to satisfy the imposed thermal boundary condition at the wall when $\sigma(\gamma-1)M^2 \lesssim O(E^{1/3})$.

First, it is shown here that no z-independent (two-dimensional) flow is allowed if $\sigma(\gamma-1)M^2 \lesssim O(E^{1/3})$. For this purpose, a z-independent flow on the $(r-\theta)$-plane is assumed, which will be shown to be incompatible with the assumptions adopted.

From (2)–(6), the z-independent (two-dimensional) leading-order equations in the interior for non-axisymmetric components, when $E \ll 1$, are

$$\frac{\partial}{\partial r}(r\rho_{00}\tilde{u}_i) + \frac{\partial}{\partial \theta}(\rho_{00}\tilde{v}_i) = 0, \tag{28a}$$

$$-2\rho_{00}\tilde{v}_i - \gamma M^2 r\tilde{\rho}_i + \frac{\partial \tilde{p}_i}{\partial r} = 0, \tag{28b}$$

$$2\rho_{00}\tilde{u}_i + \frac{1}{r}\frac{\partial \tilde{p}_i}{\partial \theta} = 0, \tag{28c}$$

$$\frac{\sigma(\gamma-1)}{\gamma} r\rho_{00}\tilde{u}_i + E\nabla^2\tilde{T}_i = 0, \tag{28d}$$

$$\tilde{p}_i = \tilde{\rho}_i + \rho_{00}\tilde{T}_i, \tag{28e}$$

in which subscript i refers to the interior variables.

From (28a)–(28c), we have

$$\frac{\partial \tilde{\rho}_i}{\partial \theta} = 0. \tag{29}$$

Since $\tilde{\rho}_i$ is a non-axisymmetric quantity, (29) indicates

$$\tilde{\rho}_i = 0. \tag{30}$$

It then follows, from (28e) and (30), that

$$\tilde{p}_i = \rho_{00}\tilde{T}_i. \tag{31}$$

In view of (28c) and (31), we obtain

$$\tilde{u}_i = -\frac{1}{2r}\frac{\partial \tilde{T}_i}{\partial \theta}. \tag{32}$$

Notice that, in the present analysis, the interior temperature field has to satisfy the boundary condition at the wall ($r=1$) because there is no thermal boundary layer of $O(1)$. Consequently, in view of (32), the leading-order interior temperature of $O(1)$, which is linked to the radial velocity $\tilde{u}_i$ of $O(1)$, is not compatible with the non-permeable radial-velocity condition at the wall, because $\partial\tilde{T}_i/\partial\theta \neq 0$ at $r=1$.

In summary, it is asserted that, in the parameter range $\sigma(\gamma-1)M^2 \lesssim O(E^{1/3})$, the above-described $E^{1/3}$-thermal layer does not exist. It follows that the effect of thermal loading at the wall diffuses into the interior, but it is not possible to have two-dimensional flows in the $(r-\theta)$-plane.

Further physical meaning may be extracted by working out an example. Consider a heavy gas for which $(\gamma-1) \ll O(E)$ and $M \sim O(1)$, and as the thermal boundary condition, the non-axisymmetric temperature distribution, $\tilde{T}_w = \sin(2\theta)$, is imposed at the wall ($r=1$). As shown in (28d), the leading-order temperature has to satisfy the diffusion equation if a two-dimensional flow in the $(r-\theta)$-plane is assumed. The solution for leading-order temperature is, from (28d),

$$\tilde{T}_i = r^2 \sin(2\theta). \tag{33a}$$

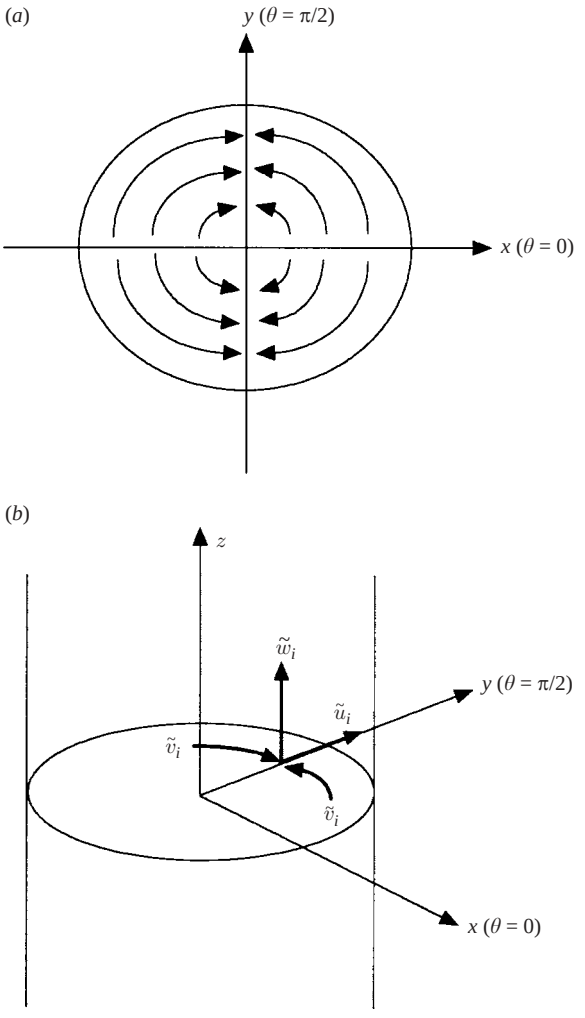

FIGURE 5. Flow patterns, (*a*) on the $(r-\theta)$-plane; (*b*) a perspective view.

From (28*b*), (28*e*), (30) and (33*a*), the leading-order solution for azimuthal velocity in the interior is acquired, i.e.

$$\tilde{v}_i = (r + \gamma M^2 r^3)\sin(2\theta), \tag{33b}$$

and, from (32) and (33*a*), the radial velocity is

$$\tilde{u}_i = -r\cos(2\theta). \tag{33c}$$

These results are demonstrated in figure 5(*a*). In the wall sector of heating [$\tilde{T}_w > 0$, i.e. $0 < \theta < \pi/2, \pi < \theta < 3\pi/2$], $\tilde{v}_i > 0$; and in the wall sector of cooling [$\tilde{T}_w < 0$, i.e. $\pi/2 < \theta < \pi, 3\pi/2 < \theta < 2\pi$], $\tilde{v}_i < 0$. Consider a $z =$ constant plane. As is discernible in figure 5(*a*), in order to maintain the azimuthal flows of (33*b*), fluid motions are directed toward (away from) the radial line of $\theta = \pi/2$ ($\theta = 0$). Since the motions have been assumed to be two-dimensional in the $(r-\theta)$-plane, $\tilde{v}_i \sim O(1)$ from (33*b*), and this points to the interior radial velocity $\tilde{u}_i \sim O(1)$ given in (33*c*). However, this result leads to a contradiction: $\tilde{u}_i \sim O(1)$ cannot satisfy the non-permeability boundary condition with any types of boundary layer. This can be explained by noting that,

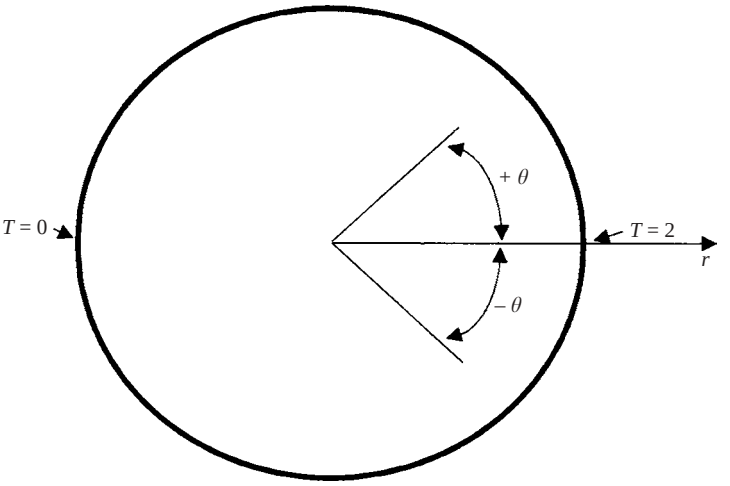

FIGURE 6. Configuration of the differential heating problem.

under the presence of a boundary layer of thickness $O(E^n)$, where $n > 0$, the radial velocity that can be matched is $O(E^n)$.

As is clear in (33*c*), the flux of fluid that is carried in by azimuthal velocities cannot be squeezed out in the radial direction; therefore, there should be a z-directional flow $\tilde{w}_i$ (see figure 5*b*). These arguments indicate the inappropriateness of the basic assumption of two-dimensionality of flow in the $(r-\theta)$-plane.

In conclusion, for $\sigma(\gamma-1)M^2 \lesssim O(E^{1/3})$, no z-independent (two-dimensional) solution exists in response to the non-axisymmetric, z-independent thermal forcing at the wall. In realistic situations, fully three-dimensional z-dependent flows are obtained. Detailed aspects of these flows are beyond the scope of the present paper.

4. Illustrative example – a differential heating on the pipe wall

As a specific and instructive example, under $\sigma(\gamma-1)M^2 \gg O(E^{1/3})$, consider a rapidly rotating pipe, with the coordinate frame attached, as displayed in figure 6. The thermal forcing at the wall is $T=0$ at $\theta=\pi$ and $T=2$ at $\theta=0$. If the wall is perfectly conducting, the temperature boundary condition is a linear function of θ. The associated boundary conditions are

$$u = v = 0, \quad T = 2\left(1 - \left|\frac{\theta}{\pi}\right|\right), \quad (-\pi < \theta \leqslant \pi) \quad \text{at } r = 1. \tag{34}$$

With the aid of the developments in previous sections, the solution is readily obtained:

$$\Phi_s(r, \zeta, \theta) = \hat{\Phi}_s(r) + \tilde{\Phi}_s(\zeta, \theta), \tag{35}$$

in which Φ_s denotes the steady flow variables such as velocities, temperature, density and pressure, a circumplex denotes the axisymmetric part and a tilde the non-axisymmetric part.

For this example, the coefficients in the previous analysis are determined as

$$\hat{f} = 1,$$

$$\tilde{f}_n = \left(\frac{2}{n\pi}\right)^2 [1-(-1)^n] \quad (n = 1, 2, 3, \ldots).$$

The temperature is,

$$T = \hat{T}_s + \tilde{T}_s = 1 + \sum_{n=1}^{\infty} \frac{2(1-(-1)^n)}{(n\pi)^2} \left[\exp(-\gamma_n \zeta) + \exp\left(-\tfrac{1}{2}\gamma_n \zeta\right) \frac{2}{\sqrt{3}} \cos\left(\frac{\sqrt{3}}{2}\gamma_n \zeta - \frac{\pi}{6} \right) \right] \cos(n\theta), \tag{36}$$

in which $\hat{T}_s$ was defined in (12) and $\tilde{T}_s$ in (24), and $\gamma_n = (\sigma(\gamma-1)M^2 n^2)^{1/6}$ and $\zeta = (1-r)/E^{1/3}$.

The density is found to be

$$\rho = \hat{\rho}_s + \tilde{\rho}_s = \frac{1}{2}\left(\frac{\gamma M^2}{1-\exp(-\gamma M^2/2)} - 2 - \gamma M^2 r^2 \right) \rho_{00}(r) - \sum_{n=1}^{\infty} \frac{2(1-(-1)^n)}{(n\pi)^2} \times \left[\exp(-\gamma_n \zeta) + \exp\left(-\tfrac{1}{2}\gamma_n \zeta\right) \frac{2}{\sqrt{3}} \cos\left(\frac{\sqrt{3}}{2}\gamma_n \zeta - \frac{\pi}{6} \right) \right] \cos(n\theta), \tag{37}$$

in which $\hat{\rho}_s$ from (15) and $\tilde{\rho}_s = -\tilde{T}_s$ from (20*e*).

From (10) and (26), the radial velocity is

$$u = \hat{u}_s + \tilde{u}_s = \frac{-\gamma E^{1/3}}{\sigma(\gamma-1)} \sum_{n=1}^{\infty} \frac{2\gamma_n^2 (1-(-1)^n)}{(n\pi)^2} \times \left[\exp(-\gamma_n \zeta) + \frac{2}{\sqrt{3}} \exp(-\gamma_n \zeta/2) \sin\left(\frac{\sqrt{3}}{2}\gamma_n \zeta - \frac{\pi}{3} \right) \right] \cos(n\theta), \tag{38}$$

and, from (11) and (27), the azimuthal velocity is

$$v = \hat{v}_s + \tilde{v}_s = \frac{\gamma}{\sigma(\gamma-1)} \sum_{n=1}^{\infty} \frac{2\gamma_n^3 (1-(-1)^n)}{(n\pi)^2} \times \left[\exp(-\gamma_n \zeta) + \frac{2}{\sqrt{3}} \exp(-\gamma_n \zeta/2) \sin\left(\frac{\sqrt{3}}{2}\gamma_n \zeta - \frac{2\pi}{3} \right) \right] \sin(n\theta). \tag{39}$$

The above theoretical results are shown graphically in figure 7. In the interior region far away from the wall, the temperature is $T = 1.0$, which is the average value of the wall temperature profile. In the $E^{1/3}$-thermal layer close to the wall, owing to the diffusion from the wall, there is a relatively hot region ($T > 1.0; -\pi/2 < \theta < \pi/2$) and a relatively cold region ($T < 1.0; -\pi < \theta < -\pi/2, \pi/2 < \theta < \pi$), which are displayed in figure 7(*a*). In the hot region ($-\pi/2 < \theta < \pi/2$), the fluid undergoes thermal expansion, which gives rise to radially inward motions. In the cold region ($-\pi < \theta < -\pi/2$, $\pi/2 < \theta < \pi$), the fluid experiences thermal compression, which causes radially-outward motions. These are illustrated in figure 7(*c*). In the course of these motions, density becomes relatively lower (higher) in the hot (cold) region, as indicated in (37) and shown in figure 7(*b*). These give rise to density variations in the azimuthal direction. It should be mentioned that, owing to the temperature increment in the whole region of the $E^{1/3}$-thermal layer near the wall (see figure 7*a*), the density field is negative in that region, i.e. $-\pi < \theta < \pi$ and $\zeta \sim O(1)$; however, it becomes positive in the interior region, i.e. $\eta \to \infty$, to satisfy global mass continuity as shown in figure 2.

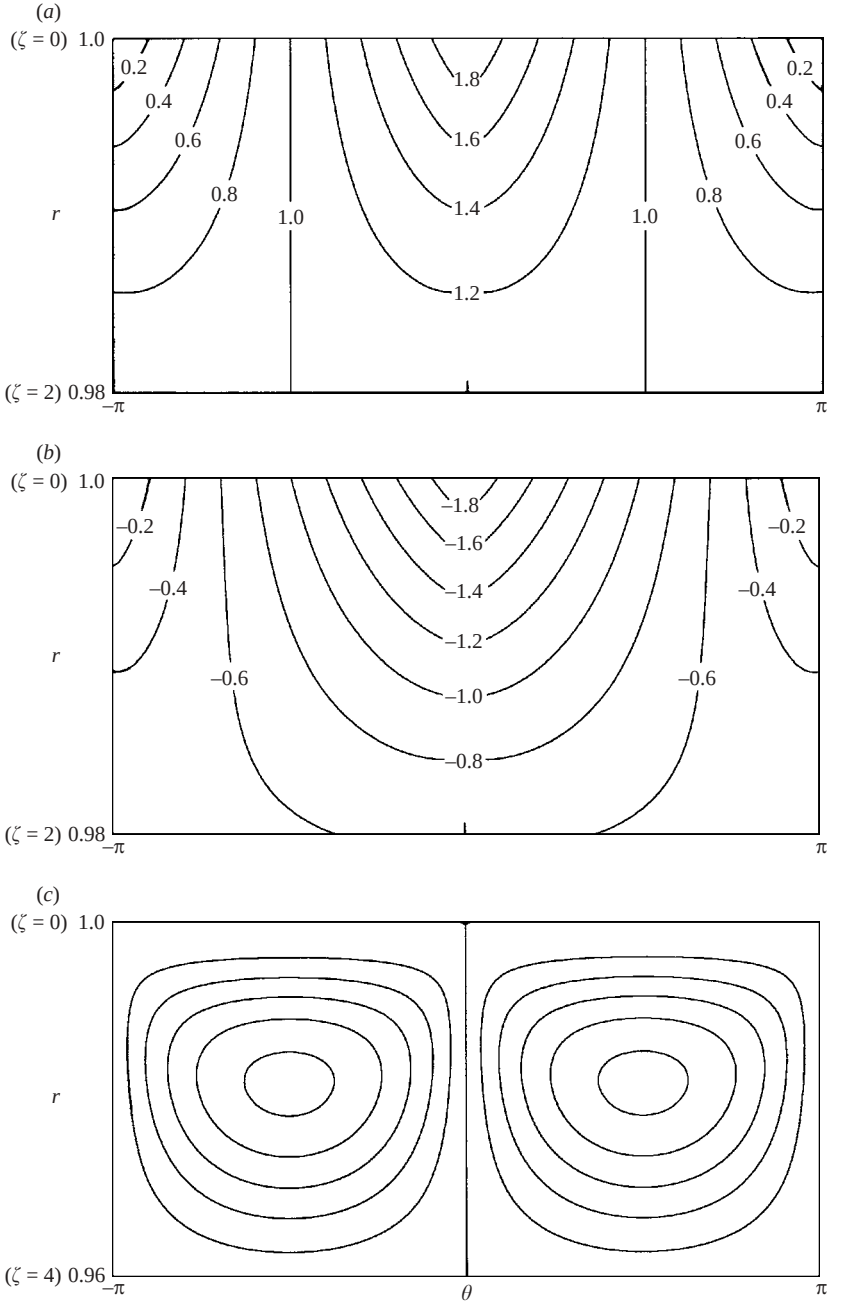

FIGURE 7. Plots of (*a*) temperature field $T = \hat{T}_s + \tilde{T}_s$; (*b*) density field $\rho = \hat{\rho}_s + \tilde{\rho}_s$ and (*c*) streamfunction $\Psi = \int \tilde{u}_s \, \mathrm{d}\theta$ near the wall. $E = 10^{-6}$, $M = 3.0$, $\gamma = 1.4$ and $\sigma = 0.7$. $\Delta\Psi = 0.2$.

Consequently, as can be inferred from (20*b*), azimuthal velocities are induced, which satisfies the geostrophic thermal wind relation. These activities are represented in the closed circulation, which is shown in figure 7(*c*).

At locations which are a distance of $O(E^{1/3})$ away from the wall, the aforestated two effects (thermal diffusion effect from the wall and thermal compression or expansion

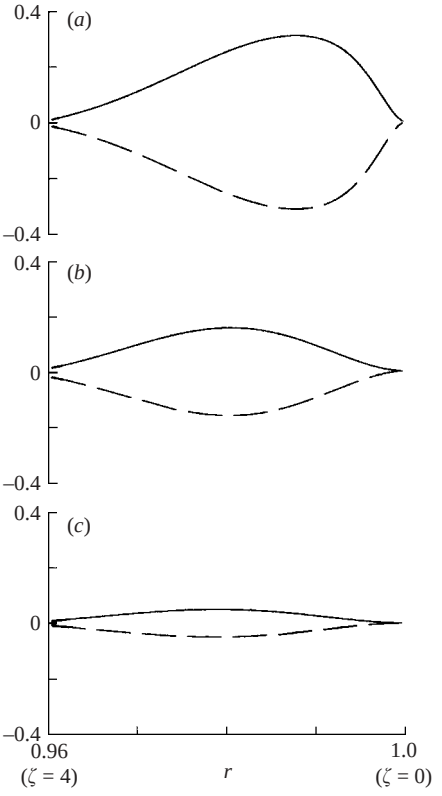

FIGURE 8. Comparisons between the radial thermal diffusion term, $E(\partial^2 T/\partial r^2)$, and the radial compression work, $(\sigma(\gamma-1)/\gamma)r\rho_{00}u$, near the wall. $E=10^{-6}$, $M=3.0$, $\gamma=1.4$ and $\sigma=0.7$. (*a*) $\theta=0$ (or π); (*b*) $\theta=\pi/5$ (or $4\pi/5$); (*c*) $\theta=2\pi/5$ (or $3\pi/5$). The solid (dashed) lines denote the radial diffusion term (radial compression work) for $\theta=0$, $\pi/5$, $2\pi/5$. For $\theta=3\pi/5$, $4\pi/5$, π, the solid (dashed) lines denote the radial compression work (radial diffusion term).

effect by the radial motion of the fluid) on the change of fluid temperature are comparable and counteracting. Therefore, the fluid temperature increase (decrease) caused by thermal diffusion from the hot (cold) sector of the wall is offset by the cooling (heating) effect from volume change of fluid which occurs due to the radially inward (outward) motions. Resultantly, at the edge of $E^{1/3}$-layer, the temperature approaches the average wall temperature $T=1.0$ which is equalized to the interior temperature. In the region of the $E^{1/3}$-layer, i.e $\zeta \sim O(1)$, the energy balance should be, from (6),

$$-\frac{\sigma(\gamma-1)}{\gamma}u \sim E\frac{\partial^2 T}{\partial r^2} + \text{higher-order terms.}$$

The above assertion is shown in figure 8, in which a diagnostic analysis between the thermal diffusion and the radial compression work terms is given. As expected from the temperature field and fluid motion given in figure 7(*a*) and 7(*c*), the radial thermal diffusion and radial compression work are most pronounced at $\theta=0$ and $\theta=\pi$ (see figure 8*a*), and those become negligible as $\theta \to \pm\pi/2$ (see figure 8*c*).

It is emphasized that, when $E \ll 1$ and $\sigma(\gamma-1)M^2 \gg O(E^{1/3})$, the fluid in the bulk of the interior maintains axisymmetric rigid-body rotation. Only inside the

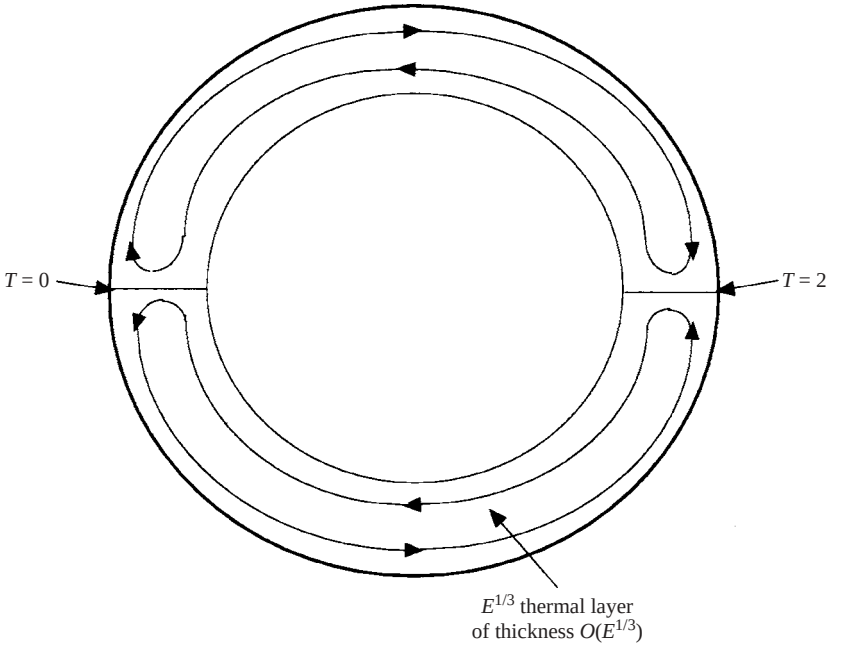

FIGURE 9. Flow patterns for the differential-heating problem.

$E^{1/3}$-thermal layer close to the wall, are flows present. Figure 9 displays the schematics of these theoretical analyses.

In summary, the temperature in the bulk of the interior is equalized to $T = 1.0$, which is the average value of temperature distribution at the wall. The temperature field is θ-dependent only inside the $E^{1/3}$-thermal layer, as given in (36). The principal dynamical balance in the interior is between the Coriolis force and the radial pressure gradient, which is embodied in the geostrophic balance. In the $E^{1/3}$-layer, balance is maintained between the Coriolis force, the radial pressure gradient, and the buoyancy resulting from the density gradient in the azimuthal direction, which is termed the thermal geostrophic wind relation.

The physical rationalizations rendered in the above for a compressible fluid are in contrast to the case of a conventional incompressible fluid. In the latter, the energy equation represents a simple diffusion process; therefore, the non-axisymmetric thermal forcing at the wall causes a corresponding non-axisymmetric temperature field in the interior. The main difference in the temperature field in the interior between compressible and incompressible fluids, subjected to the azimuthally varying temperature distribution at the wall, is exemplified in figure 10.

5. Conclusions

The axisymmetric part of the thermal forcing at the wall gives rise to the interior temperature, which is equalized to the average value, $\hat{T}_w$, of the temperature distribution at the wall. The attendant flow in the interior is in rigid-body rotation, rotating together with the pipe. In comparison with the original basic state, the density increases (decreases) in the interior region near the axis for $\hat{T}_w > 0$ ($\hat{T}_w < 0$). Near the wall, density decreases (increases) for $\hat{T}_w > 0$ ($\hat{T}_w < 0$). The pressure increases (decreases) in the entire domain for $\hat{T}_w > 0$ ($\hat{T}_w < 0$).

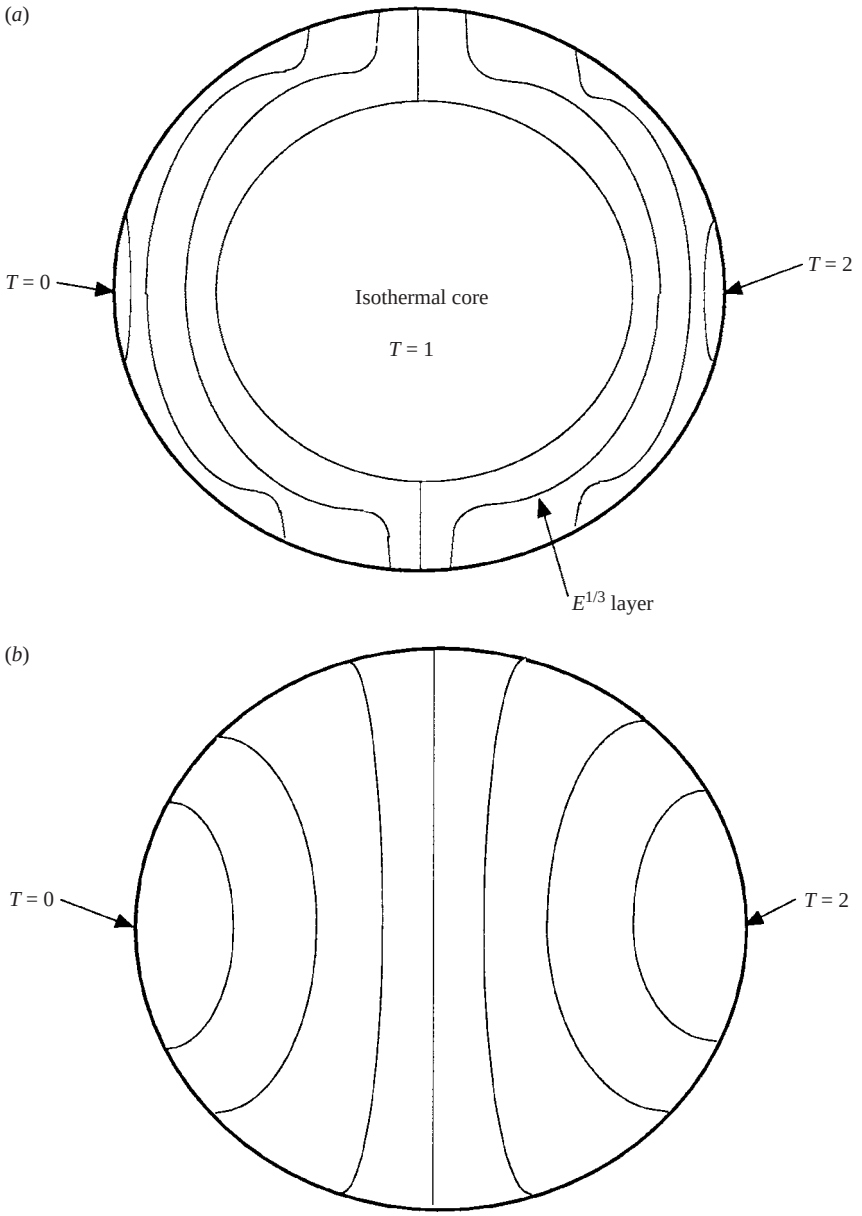

FIGURE 10. Isothermal patterns. (*a*) a compressible fluid; (*b*) an incompressible fluid.

Under a z-independent non-axisymmetric thermal forcing at the wall, in the parameter range $\sigma(\gamma - 1)M^2 \lesssim O(E^{1/3})$, it is not possible to have a z-independent (two-dimensional) flow in the $(r - \theta)$-plane.

In the parameter range $\sigma(\gamma - 1)M^2 \gg O(E^{1/3})$, the non-axisymmetric thermal forcing at the wall is absorbed in the $E^{1/3}$-thermal layer close to the wall. In the $E^{1/3}$-layer, regions of unequal temperatures, deviating from the average value $\hat{T}_w$, are formed owing to thermal diffusion from the wall. The accompanying azimuthally varying density field gives rise to a closed circulation, which is in accord with the thermal geostrophic wind relation. The attendant radial motions cause volume changes of

fluid, which bring forth an effective heating or cooling of the fluid. In the vicinity of the edge of the $E^{1/3}$-layer, the above two effects stemming from the non-axisymmetric thermal loading are comparable and counteracting; therefore, the temperature in the interior is axisymmetric and is equalized to $\hat{T}_w$.

This work was supported in part by an International Cooperative Grant from the Korea Science and Engineering Foundation (KOSEF), 2002–2004, South Korea.

REFERENCES

Babarsky, R. J., Herbst, I. W. & Wood III, H. G. 2002 A new variational approach to gas flow in a rotating system. *Phys. Fluids* **14**, 3624–3640.

Bark, F. H. & Bark, T. H. 1976 On vertical boundary layers in a rapidly rotating gas. *J. Fluid Mech.* **78**, 815–825.

Bark, F. H. & Hultgren, L. S. 1979 On the effects of thermally insulating boundaries on geostrophic flows in rapidly rotating gases. *J. Fluid Mech.* **95**, 97–118.

Batchelor, G. K. 1967 *An Introduction to Fluid Dynamics*. Cambridge University Press.

Carslaw, H. S. & Jaeger, J. C. 1959 *Conduction of Heat in Solids*. Oxford University Press.

Franlel, L. E. 1959 A cylindrical sound pulse in a rotating gas. *J. Fluid Mech.* **11**, 637–649.

Gans, R. F. 1974 On the Poincaré problem for a compressible medium. *J. Fluid Mech.* **62**, 657–675.

Gans, R. F. 1975 On the stability of shear flow in a rotating gas. *J. Fluid Mech.* **68**, 403–412.

Heijst, G. J. F. 1983 The shear-layer structure in a rotating fluid near a differentially rotating sidewall. *J. Fluid Mech.* **130**, 1–12.

Hyun, J. M. & Park, J. S. 1989 Some aspects of compressible Rayleigh's problem in a rotating cylinder. *J. Phys. Soc. Japan* **58**, 159–166.

Lalas, D. P. 1975 The 'Richardson' criterion for compressible swirling flows. *J. Fluid Mech.* **69**, 65–72.

Louvet, P. & Durivalt, J. 1977 Compressible countercurrent flow in a strongly rotating cylinder, *Singular Perturbations and Boundary Layer Theory* (ed. C. M. Brauner, B. Gay & J. Mathieu) Lecture Notes in Mathematics, vol. 594, p. 312. Springer.

Matsuda, T. 1983 Meteorology in a space colony. *J. Phys. Soc. Japan* **52**, 1904–1907.

Matsuda, T. & Hashimoto, K. 1976 Thermally, mehanically or externally driven flows in a gas centrifuge with an insulated horizontal end plates. *J. Fluid Mech.* **78**, 337–354.

Matsuda, T., Hashimoto, K. & Takeda, H. 1976 Thermally driven flow in a gas centrifuge with an insulated side wall. *J. Fluid Mech.* **73**, 389–399.

Matsuda, T. & Nakagawa, K. 1983 A new type of boundary layer in a rapidly rotating gas. *J. Fluid Mech.* **126**, 431–442.

Miles, J. W. 1981 Waves in a rapidly rotating gas. *J. Fluid Mech.* **107**, 487–497.

Morton, J. B. & Shaughnessy, E. J. 1972 Waves in a gas in solid-body rotation. *J. Fluid Mech.* **56**, 277–286.

Nakayama, W. & Usui, S. 1974 Flow in rotating cylinder of a compressible fluid. *J. Nucl. Sci. Technol.* **11**, 242–262.

Park, J. S. & Hyun, J. M. 1989 Transient adjustment of a gas contained in a rapidly-rotating infinite cylinder. *J. Phys. Soc. Japan* **58**, 3949–3959.

Park, J. K. & Hyun, J. M. 1990 Numerical solutions for thermally driven compressible flows in a rapidly rotating cylinder. *Fluid Dyn. Res.* **6**, 139–153.

Park, J. S. & Hyun, J. M. 2001 Transient response of a compressible fluid in a rapidly-rotating circular pipe. *J. Fluid Mech.* **427**, 275–297.

Sakurai, T. & Matsuda, T. 1974 Gasdynamics of a centrifugal machine. *J. Fluid Mech.* **62**, 727–736.

Torri, S. & Yang, W. J. 1994 A numerical analysis on flow and heat transfer in the entrance region of an axially rotating pipe. *ISROMAC-5, Hawaii, USA* (ed. J. H. Kim & W. J. Yang), vol. A, pp. 593–605.

Wood, H. G. & Barbarsky, R. 1992 Analysis of a rapidly rotating gas in a pie-shaped cylinder. *J. Fluid Mech.* **239**, 249–271.